JOURNAL OF MATERIALS SCIENCE **37** (2002) 1067–1075

Characteristics of powder and sintered bodies of hydrothermally synthesized Mn-Zn ferrites

WEN-HAO LIN
Department of Mechanical Engineering, Far East College, Tainan, Taiwan, ROC

CHII-SHYANG HWANG*
Department of Materials Science and Engineering, National Cheng Kung University, Tainan, Taiwan, ROC
E-mail: cshwang@mail.ncku.edu.tw

To improve the sinterability of powders fabricated by the conventional mixed-oxides method, ultrafine Mn-Zn ferrite powders were hydrothermally synthesized from metal nitrates solution using ammonia as a precipitant. The *R* value (alkalinity) was introduced to adjust the amount of added OH^- in the reaction suspension. The characteristics of the powders synthesized at different hydrothermal conditions and the properties of the sintered bodies were investigated. The results show that the *R* value and hydrothermal time have a great effect on the compositions and phases of hydrothermally synthesized Mn-Zn ferrite powders. Powders synthesized from a starting suspension with a higher content of Zn ions (or lower content of Mn^{2+}) may approach to a stable spinel structure with a lower Mn/Zn ratio as the hydrothermal time is longer. Factors affecting the position of the diffraction angle (2θ) of the spinel Mn-Zn ferrite (311) of powders may include both the compositions of spinel ferrite structure and crystallite sizes (or particle sizes) of powders. Some possible reasons were suggested to explain the dependence of composition and phase of hydrothermally synthesized Mn-Zn ferrite powders on the *R* value and hydrothermal time. The temperature that the green compact begins to shrink at increases with increasing *R* value, and ranges from 510°C ($R = 2$) to 650°C ($R = 6$). After being sintered at 950°C for 2 h in N_2 atmosphere, the relative sintered density of each specimen reaches a value of 94.5–99.8%.

1. Introduction

Mn-Zn ferrites are extensive applied in power transformer, choke coil, noise filter and other electronic components due to their high initial permeability (μi), high saturation magnetization (Bs) and low magnetic loss at high frequency [1–3]. In general, the powders are fabricated by mixed-oxides method. This method for the preparation of ferrites with a typical porosity of 7–25% [4–6] involving high temperature (1250°C–1350°C) under controlled oxygen atmospheres can result in the loss of their fine particle nature. The main advantage of this method is low production cost. However, it also has the problem of inevitable chemical inhomogeneity and contaminations during processing and the need of high temperature (1250°C–1350°C) sintering.

Recently, ferrites have been developed to meet a demand for the miniaturization of electronic components. During the manufacture of multilayer chip and LC filter, ferrite powder needs to be sintered <950°C in order to co-heat with silver internal electrodes ($T_m \cong 962$°C) [7, 8]. In the fabrication of read/write heads for high-speed magnetic recording, it requires sintered body with high-density, low-porosity (<0.3%) and high permeability [9, 10]. Therefore, powders prepared by conventional mixed-oxides method is not capable of applying in the above applications due to its higher sintering temperature and higher porosity after sintering. To circumvent those discrepancies of powders fabricated by mixed-oxides method, several wet chemical methods [11–19] have been developing for the preparation of fine ferrite powder, including hydrothermal synthesis [14–19].

Using hydrothermal method to prepare ferrite powders, literature [14–17] have focused on studying the influence of processing parameters (i.e., the pH value of the suspension, the temperature, and the time of synthesis) on the yield, composition, homogeneity and morphology of ferrite powder. The authors of this article have qualitatively studied the effects of alkalinity of starting suspensions and hydrothermal time on phases, spinel ratio and crystallite size of hydrothermally synthesized Mn-Zn ferrite powders [18]. However, the characteristics variation (phases, compositions and position of diffraction angle of spinel ferrite) of

*Author to whom all correspondence should be addressed.

powder synthesized at different contents of Zn and Mn ions of starting suspension under different hydrothermal time were seldom investigated. The purpose of this work was to study the above phenomena. Additionally, the sinterability of powders synthesized at different R values (alkalinity) and properties of sintered bodies (phases and spinel ratio) were also investigated.

2. Experimental procedure

2.1. Sample preparation

Two series of powders aimed to have the compositions of 52.9 $Fe_2O_3 \cdot 34.3$ $MnO \cdot 12.8$ ZnO and 52.7 $Fe_2O_3 \cdot 26.7$ $MnO \cdot 20.6$ ZnO (in mole%), denoted as A1, A2, respectively, were synthesized under mild hydrothermal conditions (150°C for 0–16 h) by coprecipitation from metal nitrates with aqueous ammonia. $Fe(NO_3)_3 \cdot 9H_2O$, $Mn(NO_3)_2 \cdot 4H_2O$, and $Zn(NO_3)_2 \cdot 6H_2O$ were dissolved in de-ioned water individually to have a concentration of 1 mole/L, 0.5 mole/L and 0.5 mole/L, respectively. Stoichiometric amounts of the appropriate nitrate solutions were added slowly into a teflon cup and stirred for 5 minutes. The resulted solution was then mixed with diluted aqueous ammonia under stirring. The suspension volumes were in a range of 750–850 ml. In this study, R value (alkalinity) = (moles of added OH^-) / [(moles of added Zn^{2+}) $\times 2$ + (moles of added Mn^{2+}) $\times 2$ + (moles of added Fe^{3+}) $\times 3$] was introduced to adjust the amount of added OH^- in the reaction suspension, and the R value was between 2 and 6. The details of this procedure are published elsewhere [18].

Hydrothermally synthesized powders in this study were classified into two series. Powders synthesized under different R values but with the same hydrothermal time (=2 h) were denoted as AX-RY, and powders synthesized under different hydrothermal time but with the same R value (=3) were denoted as AX-Th, where $X = 1, 2$ corresponding to A1 and A2, respectively, $Y = 2$–6 standing for R values (alkalinity) and T being the time of hydrothermal synthesis (i.e., hydrothermal time), in which $T = 0$ means the powder product was obtained by directly centrifugation without further hydrothermal treatment.

Powders were isostatically pressed into toroidal compacts (20 mm outer and 12 mm inner diameters) at 98 MPa. Sintering was performed at 950°C for 2 h in a stream of N_2; heating and cooling rates were 6 and ≈4°C/min, respectively.

2.2. Characterization

The content of $Fe^{2+}$of hydrothermally synthesized powders was determined by titration method. The metal elements in solids were analyzed using Induction Couple Plasma (ICP, ARL 3580B). The phases of synthesized powders were identified from X-ray (XRD, SIEMENS D50) diffraction patterns. In addition, for precisely identifying the variation of diffraction angle (2θ) of spinel ferrite (311) of synthesized powders, XRD analysis was performed in a low scanning speed of 0.12°/min on powders synthesized at different hydrothermal conditions.

The crystallite sizes (or particle sizes) of manganese zinc ferrites and α-Fe_2O_3 were estimated from the breadth at the half maximum of the diffraction line (311) and (110), respectively, by means of Scherrer's equation [20]. Quartz particles (>4 μm) and α-Fe_2O_3 powder (0.9 μm) calcined at 1000°C for 1 h served as external references to correct the peak position and instrumental broadening. The spinel ratio (spinel%) is defined by following equation [21]

$$\text{Spinel\%} = \frac{I_{(\text{spinel})}}{I_{(\text{spinel})} + I_{(Fe_2O_3)}}$$

where I is the intensity of the strongest peak (spinel (311) and α-Fe_2O_3 (104)) for each compound.

Densities of sintered cores were measured by the Archimedes principle. The theoretical density of spinel ferrite was used to calculate relative green density and relative sintered density. Ferrite powders obtained from different R value have different compositions. Therefore, the theoretical densities ranging from 5.08–5.10 g/cm^3 for Mn-Zn ferrites hydrothermally synthesized at different R value are determined from their molecular weights and the lattice parameters. Powders were isostatically pressed into compacts at 98 MPa, and dilatometric curve of green compact was then obtained by performing at 950°C for 2 h using dilatometer (SETARAM, FRANCE, DHT-2050 KN) in a stream of N_2; heating rates was 6°C/min.

3. Results

3.1. Characterization of ferrite powders

3.1.1. Phases of powders

Fig. 1 shows the XRD patterns of A1-RY and A2-RY powders synthesized at different R values and 150°C/2 h. Based on the XRD patterns, only spinel phase was identified for the powders synthesized at $R = 2$ and 3, while show spinel phase and α-Fe_2O_3 peaks for the powders synthesized at $R = 4$–6. Moerover, it is noted that the peak intensity of α-Fe_2O_3 phase increases with increasing R value, which indicates that the content of α-Fe_2O_3 increases with R value.

Because XRD patterns of powders synthesized at $R = 2$, 3 only show spinel phase, the other series of powders were then synthesized at different lengths of hydrothermal time (0.5–16 h) under R value of 3 to further investigate the dependence of the phases of synthesized powders on hydrothermal time. The phases of A1-Th and A2-Th powders synthesized at different lengths of hydrothermal time were shown in Table I.

TABLE I Relation between phases, identified from X-ray diffraction patterns, and the time of hydrothermal synthesis for A1-Th and A2-Th synthesized powders

Hydrothermal time (h)	0	0.5	1	2	4	8	16
A1-Th	i.d.f	S	S	S	S + α	S + α	S + α
A2-Th	i.d.f	S + α	S + α	S	S + α	S + α	S + α

i.d.f: ill-definable spinel ferrite.
S: spinel ferrite.
α: α-Fe_2O_3.

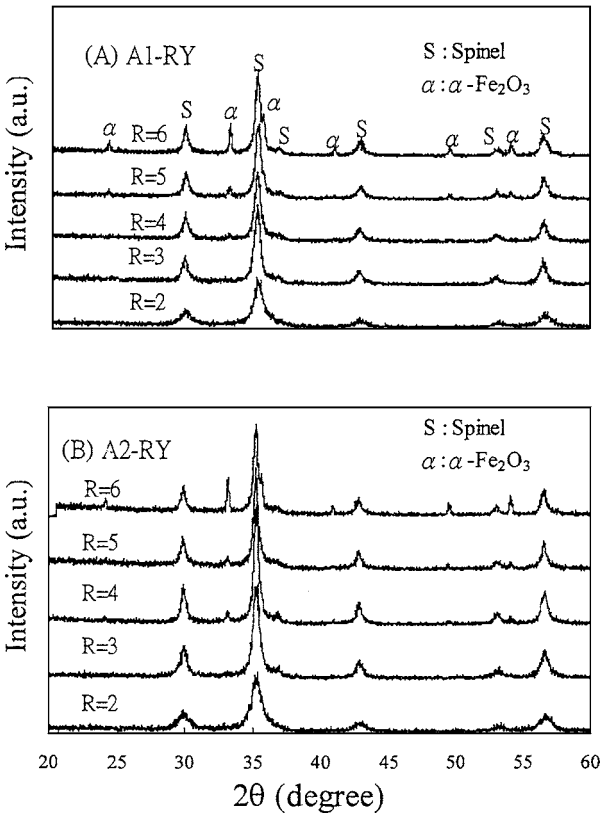

Figure 1 XRD patterns of (A) A1-R*Y*, and (B) A2-R*Y* manganese zinc ferrite powders hydrothermally synthesized at 150°C × 2 h and different *R* values (alkalinity) of reaction suspension.

The results in Table I indicate that for A1-*T*h powders, only spinel phase peak can be found in the XRD patterns of powders synthesized at hydrothermal time ≦2 h, while both the spinel phase and α-Fe_2O_3 peaks can be found in the XRD patterns of powders synthesized at hydrothermal time ≧4 h. However, for A2-*T*h series, only spinel phase is shown in the XRD pattern for A1-2h powder, while spinel phase peak and α-Fe_2O_3 peak are shown for other powders.

As above, it is noted that there are no more than two phases, spinel phase and α-Fe_2O_3, existing in powders synthesized at different hydrothermal conditions.

3.1.2. Compositions of powders

The compositions of synthesized powders described with the mole percentage of metal oxides (Fe_2O_3, MnO and ZnO) based on analytical data are shown in Table II. The [Fe_2O_3] and [MnO], molar fraction of Fe_2O_3 and MnO, respectively, in synthesized powders are larger than that in starting suspension, while the [ZnO], molar fraction of ZnO, in synthesized powders are smaller than that in starting suspension. These results indicate that Zn ions should loss during hydrothermal processing.

In order to investigate the composition difference between synthesized powders and starting suspensions, the compositions of synthesized powders were further calculated. Since the K_{sp} value (solubility product)

TABLE II Mole fractions of Fe_2O_3, MnO, ZnO, mole fraction loss of MnO and ZnO (ΔMnO, ΔZnO), crystallite sizes and spinel ratios of A1-R*Y*, A2-R*Y* powders hydrothermally synthesized at 150°C × 2 h and different *R* values (alkalinity), and A1-*T*h and A2-*T*h powders hydrothermally synthesized at 150°C for 0–16 h in *R* value (alkalinity) of 3. A1 and A2 represent the composition of starting suspensions

Sample name	Fe_2O_3 (mole%)	MnO (mole%)	ZnO (mole%)	ΔMnO (mole%)	ΔZnO (mole%)	Crystallite size (nm) α-Fe_2O_3	Crystallite size (nm) Spinel	Spinel ratio (%)
A1-R*Y* and A2-R*Y* powders (synthesized at 150°C × 2 h and different *R* values (alkalinity))								
A1	52.9	34.3	12.8					
A1-R2	54.6	33.6	11.8	1.7	1.4		10.7	100.0
A1-R3	54.4	34.7	10.9	0.5	2.2		16.5	100.0
A1-R4	56.3	36.4	7.3	0.1	5.9	49.7	18.4	89.4
A1-R5	58.1	35.5	6.4	2.0	7.0	67.2	19.5	83.7
A1-R6	59.9	36.8	3.3	1.9	9.9	72.1	20.0	73.1
A2	52.7	26.7	20.6					
A2-R2	54.3	27.4	18.3	0.1	2.8		9.7	100.0
A2-R3	54.8	28.4	16.8	−0.6	4.4		15.7	100.0
A2-R4	58.3	29.5	12.3	0.0	9.5	57.2	20.8	88.8
A2-R5	59.0	30.4	10.6	−0.5	11.1	106.3	21.4	86.5
A2-R6	61.7	32.8	5.5	−1.3	15.9	107.7	23.0	70.0
A1-*T*h and A2-*T*h powders (synthesized at 150°C for 0–16 h in *R* value (alkalinity) of 3)								
A1-0h	57.6	36.0	6.4	1.2	6.9	–	–	–
A1-0.5h	53.9	34.8	11.3	0.2	1.7	–	12.5	100
A1-1h	54.2	34.7	11.1	0.4	2.0	–	14.6	100
A1-2h	54.4	34.7	10.9	0.5	2.2	–	16.5	100
A1-4h	54.5	35.4	10.1	0.0	3.0	41.5	18.2	90.2
A1-8h	55.0	35.2	9.8	0.5	3.4	62.9	18.8	87.8
A1-16h	54.9	35.2	9.9	0.4	3.3	92.8	19.5	79.3
A2-0h	60.8	31.0	8.2	−0.2	13.5	–	–	
A2-0.5h	59.6	29.7	10.7	0.4	11.1	54.1	13.3	74.8
A2-1h	59.5	29.7	10.8	0.4	11.0	63.3	14.4	75.2
A2-2h	54.8	28.4	16.8	−0.6	4.4	–	15.3	100
A2-4h	55.8	28.2	16.1	0.1	5.4	65.2	20.0	84.1
A2-8h	59.6	29.9	10.5	0.3	11.3	224.0	23.0	69.9
A2-16h	59.5	29.8	10.8	0.3	11.0	224.0	23.0	67.7

of Fe^{3+} is very small [22], the Fe^{3+} will completely precipitate in the weakly alkaline solution. The molar fractions of MnO and ZnO in synthesized powders were then normalized by the content of Fe_2O_3. The normalization is based on the assumption that the $[Fe_2O_3]$ (in mole%) of synthesized powders are the same as that of starting suspension. Therefore, the $[\Delta MnO]$ $(=[MnO]_{\text{starting suspension}} - [MnO]_{ICP})$ and $[\Delta ZnO]$ $(=[ZnO]_{\text{starting suspension}} - [ZnO]_{ICP})$ means the loss of Mn ions loss and Zn ions loss during the hydrothermal process, respectively. The $[\Delta MnO]$ and $[\Delta ZnO]$ of A*X*-R*Y* and A*X*-*T*h synthesized powders are listed in Table II. It is noted that the $[\Delta ZnO]$ values of synthesized powders are much larger than the $[\Delta MnO]$ values, indicating that the metal ions loss during hydrothermal processing is mainly attributed to Zn ions.

As hydrothermal time is kept at 2 h, the $[\Delta ZnO]$ values of A1-R*Y* and A2-R*Y* synthesized powders increase with increasing *R* value. However, when *R* value of reaction suspension is kept at 3, the dependence of $[\Delta ZnO]$ values on hydrothermal time for A1-*T*h and A2-*T*h synthesized powders are quite different. For A1-*T*h series, the A1-0h as precipitated powder has a much larger $[\Delta ZnO]$ value (6.9 mole%) than other A1-*T*h powders (1.7–3.4 mole%). Nevertheless, the $[\Delta ZnO]$ decreases a lot to 1.7 mole%, as the hydrothermal time is 0.5 h, then increases gradually to 3.3 mole% with hydrothermal time up to 8 h. When the hydrothermal time is ≧8 h, the $[\Delta ZnO]$ values keep almost unchanged. This result may hint that the chemical reaction comes to balance at this moment.

For A2-*T*h powders, the $[\Delta ZnO]$ values are very large (13.5–11.0 mole%) for powders synthesized at hydrothermal time ≦1 h. As the hydrothermal time increases from 1 h to 2 h, the $[\Delta ZnO]$ value decreases dramatically from 11.0 to 4.4 mole%. Afterwards,the $[\Delta ZnO]$ vaiue increases to 16 mole% with increasing hydrothermal time up to 16 h.

It should be noted that starting suspension of A1 contains a much lower content of Zn ions (or higher content of Mn ions) than starting suspension of A2. As the hydrothermal time is 0.5 h, the $[\Delta ZnO]$ value (1.7 mole%) of A1-0.5h synthesized powder is much smaller than that (11.1 mole%) of A2-0.5h synthesized powder. This fact indicates that a starting suspension with a higher content of Zn ions will have more amount of Zn ions loss (larger $[\Delta ZnO]$ value) during the initial hydrothermal stage.

As mentioned above, there are no more than two phases, spinel phases and α-Fe_2O_3, existing in powders synthesized at different hydrothermal conditions (Table I and Fig. 1). The Mn and Zn elements in the powders should therefore exist in spinel ferrite. To further clarify the compositions of spinel phase in synthesized powders, the powders were analyzed to determine the content of Fe^{2+}, and the result shows that no Fe^{3+} was reduced to Fe^{2+} during powder preparation. The result hints that the spinel structure of these synthesized powders can be represented as $(Mn_xZn_{1-x})O \cdot Fe_2O_3$, which means the ratio of $([MnO] + [ZnO]) : [Fe_2O_3]$ is 1 : 1 in spinel structure. Then if $[Fe_2O_3]$, the concentration of Fe_2O_3 in synthesized powder, is more than the summation of [MnO and [ZnO] (in mole%) in synthesized powder, it would have free Fe_2O_3 $(=([Fe_2O_3] - ([MnO] + [ZnO]))$ existing in synthesized powders. The reaction scheme therefore can be written as [18]:

$$xMn^{2+} + (1-x)Zn^{2+} + (2+2y)Fe^{3+} + (8+6y)OH^- \rightarrow Mn_xZn_{1-x}Fe_2O_4 + yFe_2O_3 + (4+3y)H_2O \quad (1)$$

The x and $1-x$ values in Equation 1 mean the molar fraction of $[MnO]/([MnO] + [ZnO])$ and $[ZnO]/([MnO] + [ZnO])$ in spinel structure of synthesized powders, respectively; y value means the amount of free Fe_2O_3 existing in powder after hydrothermal process. However, it should be mentioned that the definition of x value here may be not suitable for the as precipitated powders of A1-0h and A2-0h. The composition of synthesized powders by ICP analysis were then represented as $(Mn_xZn_{1-x})O \cdot Fe_2O_3 + yFe_2O_3$ by which the x and y values of each synthesized powder can be calculated.

Dependence of x and y values on R value and hydrothermal time are shown in Fig. 2A and B, respectively. The x values (Fig. 2A) of synthesized powders increase with increasing R value for both A1 and or A2 series. This result reveals that powder synthesized at a higher R value owns a spinel structure with a larger value of Mn/Zn ratio as compared to that synthesized at a lower R value. In addition, Fig. 2A

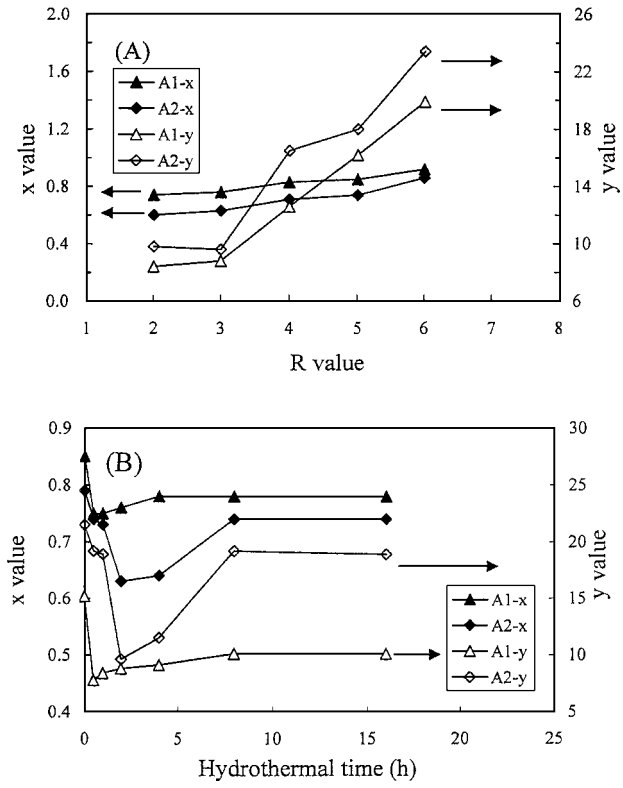

Figure 2 Dependence of x and y value on (A) R value and (B) hydrothermal time according to the powder composition definition of $(Mn_xZn_{1-x})O \cdot Fe_2O_3 + yFe_2O_3$. The powder compositions were calculated from ICP analysis data.

also shows that the y value (i.e., $[Fe_2O_3]$ in synthesized powder) increases with R value, which is consistent with the result obtained from XRD analysis (Fig. 1). Therefore, with the increase of R value, there would be more amount of Zn^{2+} ion not capable of occupying the lattice of spinel structure, and thus makes more excess amount of Fe^{3+}, not matching the stoichiometric composition of sponel ferrite, to from α-Fe_2O_3 during hydrothermal processing.

Fig. 2B shows that all the x and y values of A1-Th and A2-Th first decrease and then increase with increasing hydrothermal time. However, the amplitude of variation of x and y values for A1-Th and A2-Th powders are quite different.

For A1-Th powders, with the increase of hydrothermal time, the x and y values of synthesized powders first decrease at hydrothermal time ≦1 h, and then increase a little at hydrothermal time ≧2 h. While for A2-Th powders, as the hydrothermal time increases, the x and y values of synthesized powders first decrease at hydrothermal time ≦2 h, and then increase a lot at hydrothermal time ≧2 h. The trends of the dependence of x and y values on hydrothermal time for A1-Th and A2-Th powders are similar. However the variation of the x and y value with the increase of hydrothermal time for A2-Th powders are much larger than that of A1-Th powders. These facts indicate that hydrothermal time plays a more significant effect on the compositions of A2-Th powders. However, there exists a similar trend of x and y value variation at hydrothermal time of 8–16 h, where the x and y values of synthesized powders keep almost unchanged for both A1-Th and A2-Th powders.

Besides, it can be found that the variation of y values of synthesized powders is consistent with the result of spinel ratio of synthesized powders listed in Table II. That is the larger the y value the lower the spinel ratio of synthesized powders, indicating that the results obtained from ICP analysis match the results from XRD analysis.

3.1.3. Crystallite size of synthesized powders

The dependence of crystallite sizes of α-Fe_2O_3 and spinel ferrite in synthesized powders on the R value and hydrothermal time is shown in Table II. It is found that both the crystallite sizes of α-Fe_2O_3 and spinel ferrite increase with increasing R values. As the hydrothermal time increases, the particle sizes of α-Fe_2O_3 and spinel ferrite for both series also become larger at hydrothermal time ≦8 h , then keep almost the same. However, the particle sizes of α-Fe_2O_3 and spinel ferrite in A2-Th are larger than in A1-Th powders.

3.1.4. Variation of X-ray diffraction angle (2θ) of diffraction line (311) of spinel ferrite

XRD patterns of powders synthesized at different hydrothermal time and R value (alkalinity), in a low scanning speed of 0.12°/min are shown in Figs 3 and 4, respectively. With the increase of R value, the diffraction angle (2θ) of spinel ferrite (311) of A1-RY and A2-RY powders (i.e., only shows XRD patterns of R values of 2, 3 and 6) shifts to a low diffraction angle position (Fig. 3). Besides, the diffraction angle (2θ) of

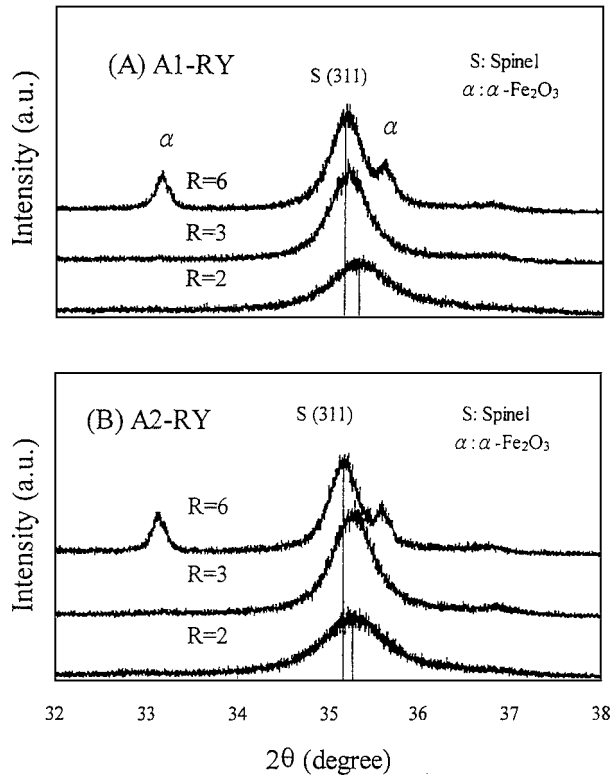

Figure 3 XRD patterns of (A) A1-RY and (B) A2-RY powders hydrothermally synthesized at 150°C × 2 h, at series R values (alkalinity) of 2, 3 and 6, in a low scanning speed (0.12°/min) of X-ray diffraction analysis.

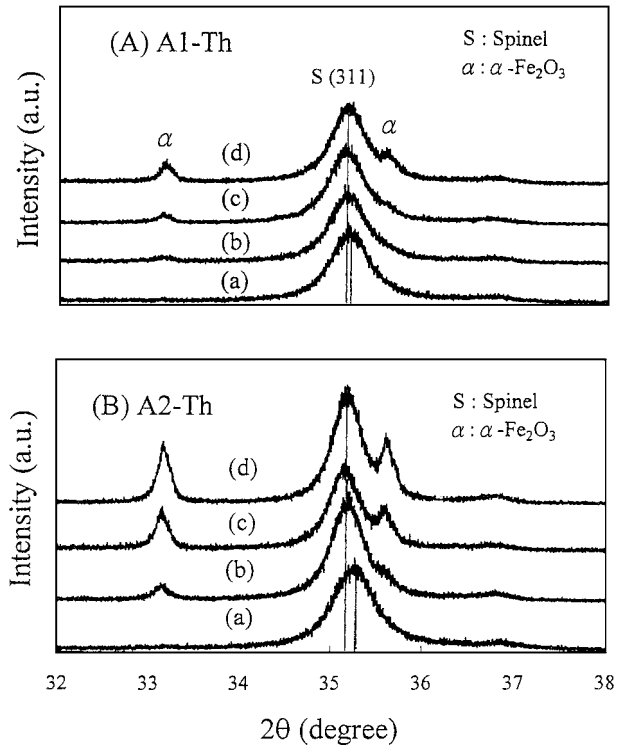

Figure 4 XRD patterns of (A) A1-Th and (B) A2-Th powders hydrothermally synthesized at 150°C with a R value (alkalinity) of 3 and at hydrothermal time of (a) 2 h, (b) 4 h, (c) 8 h, and (d) 16 h, in a low scanning speed (0.12°/min) of X-ray diffraction analysis.

TABLE III Relative green densities of A1-RY green bodies, and relative sintered densities and spinel ratios of A1-RY specimens sintered at 950°C for 2 h in N_2 atmosphere

Sample name	Spinel ratio (%)	Relative green density (%)	Relative sintered density (%)
A1-R2	91.1	41.6	94.5
A1-R3	81.1	43.2	99.8
A1-R4	71.9	43.3	96.6
A1-R5	66.8	44.8	98.4
A1-R6	54.7	48.4	99.4

spinel ferrite (311) of A1-Th and A2-Th powders also shifts to a lower angle position with the increase of hydrothermal time from 2 to 8 h, and keeps unchanged at hydrothermal time of 8–16 h (Fig. 4).

3.2. Properties of sintered bodies

Fig. 5 shows the dilatometric curves of green compacts of A1-RY specimens, performed at 950°C × 2 h in N_2 atmosphere. It is found that the temperatures that the green compacts begin to shrink at increase with increasing R values for A1-RY specimens, and range from 510°C ($R = 2$) to 650°C ($R = 6$). After being sintered at 950°C for 2 h, the shrinkage (24–20%) of each specimen decreases as the R value increases and the relative sintered density of each specimen reaches a value of 94.5–99.8%. In addition, a retardation on shrinking for the green compact of A1-R2 specimen is found at around 700°C. (i.e. possible reason will be introduced in the discussion.)

XRD patterns of A1-RY specimens, sintered at 950°C × 2 h in N_2 atmosphere are shown in Fig. 6. XRD patterns of all the A1RY-2h sintered show the existence of spinel phase and α-Fe_2O_3 peaks. Besides, the intensity of α-Fe_2O_3 peak increases with increasing R value indicating that the spinel ratios of A1-RY sintered specimens would decrease with increasing R value (Table III). Such a trend is similar to that of A1-RY synthesized powders (Table II).

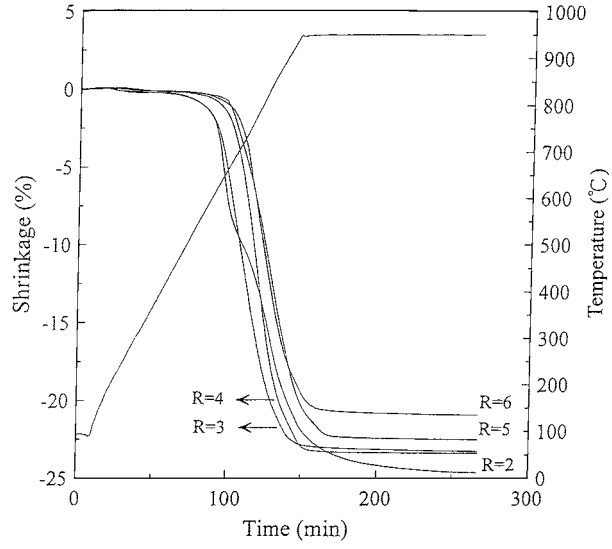

Figure 5 Dilatometric curve of A1-RY specimens, heated to 950°C and hold for 2 h, in N_2 atmosphere.

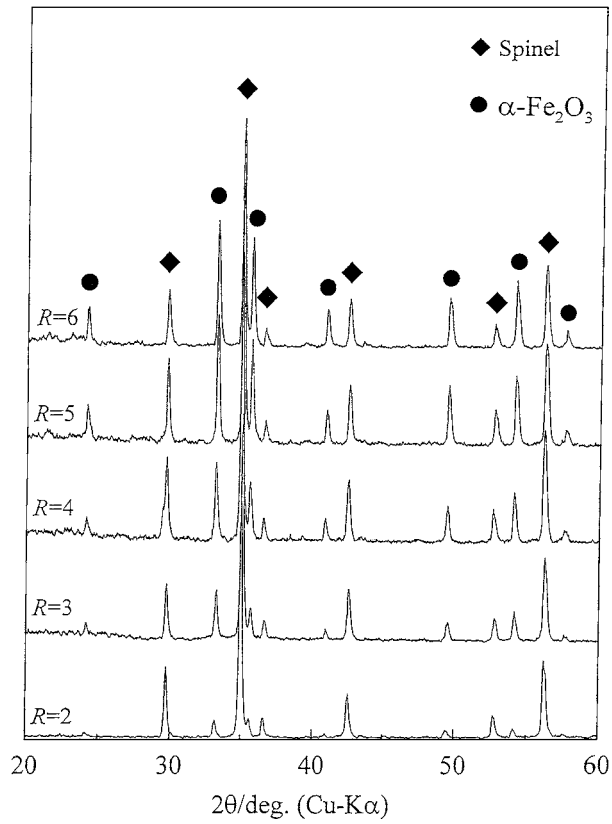

Figure 6 XRD patterns of A1-RY specimens, sintered at 950°C × 2 h in N_2 atmosphere.

4. Discussion

4.1. Powder characteristics

4.1.1. Composition and phase of synthesized powders

Based on the experimental results, it is concluded that both R value and hydrothermal time have a great effect on the composition and phase of hydrothermally synthesized manganese zinc ferrite powders. The possible reasons for the dependence of composition and phase on R value and hydrothermal time are suggested as follows.

4.1.1.1. Effect of R value. In the initial stage of hydrothermal process, the hydrothermal environment force more amount of Zn^{2+} to form $Zn(OH)_{2(s)}$, which can further react with $Mn(OH)_{2(s)}$ and $Fe(OH)_{3(s)}$ to form spinel ferrites. However, $Zn(OH)_{2(s)}$ is amphoteric and can dissolve in an excess of the base to form $Zn(OH)_4^{2-}$. The related reactions, and K_{sp} (solubility product) or K_f (formation constant) for these reactions are shown as follows.

$$Zn^{2+} + 2OH^- \rightarrow Zn(OH)_{2(s)} \quad (2)$$

$$K_{sp} = [Zn^{2+}] \cdot [OH^-]^2 = 2 \times 10^{-14}$$

$$Zn(OH)_{2(s)} + 2OH^- \rightarrow Zn(OH)_4^{2-} \quad (3)$$

$$K_f = \left[Zn(OH)_4^{2-}\right] / [OH^-]^2 = 0.13$$

$$Zn^{2+} + 4OH^- \rightarrow Zn(OH)_4^{2-} \quad (4)$$

$$K_f = \left[Zn(OH)_4^{2-}\right] / [Zn^{2+}] \cdot [OH^-]^4$$
$$= 0.13/2 \times 10^{-14} = 6.5 \times 10^{12}$$
$$xMn(OH)_{2(s)} + (1-x)Zn(OH)_{2(s)} + Fe(OH)_{3(s)}$$
$$\rightarrow Mn_xZn_{1-x}Fe_2O_4 + H_2O \quad (5)$$

where the $[Zn^{2+}]$ and $[Zn(OH)_4^{2-}]$ mean the equilibrium concentration of Zn^{2+} and $Zn(OH)_4^{2-}$ in the reaction suspension.

When the R value of starting suspension (A1 or A2) increases (i.e., a larger pH value), there would be more amounts of OH^- existing in reaction suspension during hydrothermal processing. From the equilibrium formation constant of Equation 4, it is noted that when there is more amounts of OH^- existing in reaction suspension, there would also form more amounts of $Zn(OH)_4^{2-}$ in reaction suspension during hydrothermal processing, which means more loss of Zn ions, and indicates why powders synthesized at a higher R value have a larger value of [ΔZnO] (Table II). And thus, more iron oxide present in powder synthesized at a higher R value could have originated from $Fe(OH)_{3(S)}$ that did not form ferrite because of the shortage of $Zn(OH)_{2(s)}$.

When the R value for starting suspensions of A1 and A2 is the same, the $[OH^-]$ in each reaction suspension is almost the same (i.e., the pH value for A1 and A2 reaction suspension under the same R value is nearly the same). Therefore, the ratio of $[Zn(OH)_4^{2-}]$/ $[Zn^{2+}]$ should be the same for A1 and A2 reaction suspension under the same R value (Equation 4), and hence indicates that there will be fixed ratio of $[Zn^{2+}]$ in starting suspension forming $Zn(OH)_4^{2-}$ without consolidation during hydrothermal processing. This phenomenon means that when a starting suspension having a higher $[Zn^{2+}]$ would have a larger amount of Zn ions loss during hydrothermal synthesis.

4.1.1.2. Effect of hydrothermal time. In general, the mechanism for the formation of spinel ferrite during hydrothermal synthesis is suggested as follows: metal ions in the reaction suspension form $M(OH)_x$ first, then further react with each other to yield spinel ferrites according to stoichiometric composition of $(Mn_xZn_{1-x})O \cdot Fe_2O_3$. As mentioned above, a starting suspension with a higher $[Zn^{2+}]$ will form more amount of $Zn(OH)_4^{2-}$ during reaction. The latter will lose in filtration process. Finally, the reaction system with a higher $[Zn^{2+}]$, i.e., A2-Th series, will loss more amount of Zn ions.

In a previous study [23], the formation of Mn-ferrite is found to be easier than that of Zn ferrite. Therefore, the Mn^{2+} ion may enter the lattice of spinel ferrite prior to Zn^{2+} ion during hydrothermal processing. With the increase of hydrothermal time, the Zn^{2+} ion will slowly enter into the lattice of spinel ferrite, and thus makes the [ΔZnO] value of synthesized powders to decrease with increasing hydrothermal time. However, the formed spinel ferrite maybe further reacts with OH^- [16] according to the following reaction:

$$Mn_xZn_{1-x}Fe_2O_4 + (1-x/a)OH^-$$
$$+ (1-x/a)\,H_2O \rightleftarrows (1-x/a)\,Zn(OH)_4^{2-}$$
$$+ (1-x/a)\,Fe_2O_3 + x/a\,Mn_aZn_{1-a}Fe_2O_4 \quad (6)$$

where the a value is larger than x value.

The above reaction will cause more loss of Zn ions loss and produce more amount of α-Fe_2O_3 as the hydrothermal time is longer (Table II). Hence, the α-Fe_2O_3 peak found in the XRD patterns of powders synthesized at hydrothermal time of ≦4 h can be due to more amount of α-Fe_2O_3 existing in these powders (Table II).

The reason why the formed spinel ferrite will further react with OH^- to form $Zn(OH)_4^{2-}$ and produce more amount of α-Fe_2O_3 for longer hydrothermal time can also be explained by Equation 6 as follows:

With the increase of hydrothermal time, the spinel ferrite may approach to a more stable structure (i.e., a suitable Mn/Zn ratio in spinel structure). In Equation 6, the reaction toward left means to form a spinel structure with a lower Mn/Zn ratio. On the other hand, the reaction toward right due to the formation of $Zn(OH)_4^{2-}$ means to form a spinel structure with a higher Mn/Zn ratio.

As mentioned above, with the increase of hydrothermal time, the Mn^{2+} prior to Zn^{2+} enter into the spinel structure to form manganese zinc ferrite. It is noted that A2 reaction suspension contain more amount of $Zn(OH)_4^{2-}$ as compared to A1 reaction suspension (Equation 4). According to the Equation 6, it can be understood that a reaction suspension with a higher $[Zn(OH)_4^{2-}]$ is easier to make the reaction shift toward left according to the Le Chatelier's principle, leading to that the spinel ferrite from A2 suspension is easier to react toward to the left than A1 reaction suspension. Therefore, powders synthesized from A2 suspension is tend to have lower Mn/Zn ratio than that of the spinel ferrite from A1 suspension.

Here, it can be further concluded that A2 starting suspension contains a lower amount of $[Mn^{2+}]$ (or higher amount of $[Zn^{2+}]$), so that only much lower fraction of Zn^{2+} ion in the starting suspension can enter into the lattice of spinel ferrite (i.e., as compared to A1 starting suspension) according to the final stable spinel structure. Then, more amounts of Zn^{2+} ions will loss during hydrothermal synthesis for a longer hydrothermal time (2–8 h). When the hydrothermal time increases up to ≧8 h, the compositions of both the A1-Th and A2-Th powders keep nearly unchanged, meaning that the each series of hydrothermally synthesized powders (A1-Th or A2-Th) have individually reached its final stable spinel ferrite structure at this moment.

It is noted that both the amount and particle size of α-Fe_2O_3 in AX-RY synthesized powders increase with the increase of R value. The powders synthesized at lower R values (i.e., $R = 2$ and 3) have lower amount of α-Fe_2O_3 and the particle size of α-Fe_2O_3 in AX-RY synthesized powders is smaller than that of powders synthesized at higher R values (i.e., $R = 4$, 5 and 6). Thus, no α-Fe_2O_3 peak in the XRD patterns of AX-RY powders (Fig. 1) synthesized at $R = 2$–3 and

150°C × 2 h, may be due to a lower degree of powder crystallinity and a lower amount of α-Fe_2O_3 existing in these powders.

Because the crystallite sizes of α-Fe_2O_3 and spinel ferrite of A*X*-*T*h powders increase with the increase of hydrothermal time, powders synthesized at hydrothermal time of ≦2 h own smaller particle sizes . However, it can be found that the *y* values (i.e., the content of α-Fe_2O_3 obtained from ICP analysis) of the A2-0.5h and A2-1h are obviously much larger that those of A1-0.5h and A1-1h powders. These results indicate that α-Fe_2O_3 peak appearing in the XRD patterns of A2-0.5h and A2-1h powders is mainly due to more amount of α-Fe_2O_3 existing in powders, while no α-Fe_2O_3 peak in the XRD patterns of A1-0.5h and A1-1h powders may be mainly due to a lower degree of powder crystallinity and a lower amount of α-Fe_2O_3 existing in these powders.

It should be noted that the *y* values of A1-*T*h powders synthesized at hydrothermal time ≧4 h are only a little larger that of A1-2h powder (i.e., the same as A1-R3 powder), while the *y* values of A2-*T*h powders synthesized at hydrothermal time ≧ 4 h are much larger than that of A2-2h powder (Fig. 2B). As indicated in Fig. 1, there is no α-Fe_2O_3 peak appearing in the XRD patterns of A1-2h (or A1-R3) and A2-2h (or A2-R3) powders. Therefore, the α-Fe_2O_3 peak appearing in the XRD patterns of A1-4h–A1-16h may be mainly due to their higher crystallinity of α-Fe_2O_3 powder as compared to that of A1-2h powder, while the α-Fe_2O_3 peak appearing in the XRD patterns of A2-4h–A2-16h are attributed to not only the higher crystallinity of α-Fe_2O_3 phase but indeed also more amount of α-Fe_2O_3 existing in these powders as compared to that of A2-2h powder.

4.1.2. Relation between crystallite size and the variation of X-ray diffraction angle (2θ) of diffraction line (311) of spinel ferrite

As the *R* value or hydrothermal time increases, the X-ray diffraction angles (2θ) of diffraction line (311) of spinel ferrite of synthesized powders have a trend to shift to a lower angle (Figs 3 and 4), then locates at the same position when hydrothermal time is ≧8 h. The authors of this article have proposed the shift of X-ray diffraction angles of spinel ferrite (311) for powders synthesized at different *R* values (alkalinity) may be due to different compositions of spinel structure (i.e., the composition for the spinel ferrite has changed) (Fig. 2) according to the Bragg's law. However, the shift of diffraction angles of spinel ferrite (311) may also caused by the variation of particle size of spinel ferrite. Because, when considering the relation between the particle size and diffraction angles (2θ) of line (311) of spinel ferrite of synthesized powders, it is noted that the trend of the variation for the crystallite sizes of powders is similar to that for X-ray diffraction angles (2θ) of diffraction line (311) of spinel ferrite. That is, the larger the particle size of spinel ferrite (i.e., for powders synthesized at a higher *R* value or a longer hydrothermal time) the lower the diffraction angle will be.

Therefore, it may conclude that both the composition of spinel ferrite structure and particle size of powder may cause the shift of the X-ray diffraction angle.

4.2. Properties of sintered body

The fact that the temperature for the green compact of A1-Ry beginning to shrink at increases with increasing *R* value could be attributed to the characteristic variation of the powders. It is known that the particle size of synthesized powders increases with *R* value (Table II). In general, the larger the particle sizes, the higher the sintering temperature needed for the green compact. Besides, there is more amount of α-Fe_2O_3 in the form of large grain (Table II) existing in powders synthesized at a higher *R* value. The α-Fe_2O_3 with of large grain may acts as a second phase and inhibits the initial sintering of ferrite powder within the green compact.

The result that the shrinkage of green compact of A1-R*Y* powders decreases with increasing *R* value can be attributed to difference on green density and particle size of the powder. It is found that the green densities of A1-R*Y* specimens increases with *R* value (Table III). Generally, the larger the green density, the smaller the shrinkage after sinterung. In addition, the powders synthesized at a higher *R* value has larger particle size as compared to the powders synthesized at a lower *R* value (Table II). A particle with larger size will be less active, and hence lower in sinterability. However, particles wuth smaller sizes will be easier to agglomerate, resultimg in lower density in green compact.

As shown in Fig. 5, there is retardation on shrinkage for A1-R2 specimen at around 700°C. The reason for this phenomenon is still uncertain. However, it is found that there are more amount of amine complexes and hydroxide complexes existing in A1-R2 powder than in the other powders (A1-R3–A1-R6) [19]. These impurities (amine complexes and hydroxide complexes) may decompose and inhibit the shrinkage of green compact during heating to an elevated temperature around 700°C.

The evaporation of ZnO (which decomposes to Zn and O_2) of hydrothermally synthesized powders generally occurs at temperature above 1050°C [17]. This indicates that the compositions of A1-R*Y* specimens after sintering at 950°C for 2 h would not change as compared to the corresponding synthesized powders. Therefore, The result that the spinel ratios of sintered specimen decrease with increasing *R* value (Table III) may be attributed to no composition variation after sintering.

It can be noted that XRD patterns of A1-R2 and A1-R3 powders do not show the existence of α-Fe_2O_3 peak (Fig. 1), while those of A1-R2 and A1-R3 sintered specimens show the existence of α-Fe_2O_3 peak (Fig. 6). As mentioned above, the compositions of sintered specimens should be nearly the same as that of the corresponding synthesized powders under the same *R* value due to no evaporation of ZnO during sintering. The existence of α-Fe_2O_3 peak in the XRD patterns of A1-R2 and A1-R3 sintered specimens confirms that no α-Fe_2O_3 peak appearing on the XRD patterns of A1-R2 and A1-R3 powders may be due to less powder

crystallinity, which is beyond the limitation of X-ray diffraction analysis.

5. Conclusions

(1) The *R* value and hydrothermal time have a great effect on the compositions and phases of hydrothermally synthesized manganese zinc ferrite powders, especially on powders synthesized from a starting suspension with a higher content of Zn ions.

(2) Powders synthesized from a starting suspension with a higher content of Zn ions (or lower content of Mn^{2+}) may approach to a stable spinel structure with a lower Mn/Zn ratio as hydrothermal time is longer. When the hydrothermal time increases up to $\geqq$8 h, manganese zinc ferrite powders hydrothermally synthesized from suspension containing different amount Mn^{2+} and Zn^{2+} ions have individually reached its final stable spinel structure.

(3) Factors affecting the position of diffraction angle (2θ) of the spinel Mn-Zn ferrite (311) of powders may include both the compositions of spinel ferrite structure and crystallite sizes (or particle sizes) of powders.

(4) The temperature that the green compact begins to shrink at increases with increasing *R* value, and ranges from 510°C to 650°C. After being sintered at 950°C for 2 h in N_2, the relative sintered density of each specimen reaches a value of 94.5–99.8%.

Acknowledgments

The authors are grateful to National Science Council, Republic of China, for financial support under Contract No. NSC-88-2216-E006-034.

References

1. T. SANO, A. MORITA and A. MATSUKA, in Proceedings of 3rd High Frequency Power Conversion Conference, 1988, San Diego, CA, p. 1; E. C. SNELLING, *IEEE Spectrum* **9**(1) (1972) 46.
2. P. I. SLICK, in "Ferromagnetic Materials," Vol. 2, edited by Wohlfarth (North-Holland, New York, 1980).
3. J. A. T. TAYLOR, S. T.RECZEK and A. ROSEN, *Am. Ceram. Soc. Bull.* **74**(4) (1995) 91.
4. B. B. GHATE, *Mater. Sci. Res.* **11** (1978) 369.
5. P. K. GALLAGHER, E. M. GYORGY, D. W. JOHNSON, W. DAVID, M. ROBBINS and E. M. VOGEL, *J. Amer. Ceram. Soc.* **66** (7) (1983) C110.
6. E. HIROTA, K. HIROTA and K. KUGIMIYA, in Ferrites, Proc. Int. Conf. (University of Tokyo, Tokyo, 1980) p. 667.
7. K. Y. KIM, W. S. KIM, Y. D. JU and H. J. JUNG, *J. Mater. Sci.* **27**(17) (1992) 4741.
8. M. FUJIMOTO, *J. Amer. Ceram. Soc.* **77**(11) (1994) 2873.
9. J. KULIKOWSKI and A. LESNIEWSKI, *J. Magn. Magn. Mater.* **19** (1980) 117.
10. H. IGARSHI and K. OKAZAKI, *J. Amer. Ceram. Soc.* **60**(1) (1977) 51.
11. B. F. B. YU and A. GOLDMAN, in Ferrites, Proc. ICF, 3rd. ed., edited by H. Watanabe, S. Iida and M. Sugimoto (Center for Academicc Press, Tokyo, Japan, 1982) p. 68.
12. T. PANNAPARAYIL, R. MARANDE and S. KOMARNENI, *J. Appl. Phys.* **69**(8) (1991) 5349.
13. H. B. BEER, F. A. M. VAN DEN KEYBUS and L. F. SUYKERBUYK, *PCT International* Patent (US), WO 8,301,464 A1 (1983).
14. W. J. DAWSON, *Am. Ceram. Soc. Bull.* **67**(19) (1988) 1673.
15. S. KOMARNENI, E. FRAGEAN, E. BREVEL and R. ROY, *J. Amer. Ceram. Soc.* **71**(1) (1988) C-26.
16. M. ROZMAN and M. DROFENIK, *ibid.* **78**(9) (1995) 2449.
17. *Idem.*, *ibid.* **81**(7) (1998) 1757.
18. W. H. LIN, S. K. JANG JEAN and C. S. HWANG, *J. Mater. Res.* **14** (1) (1999) 204.
19. *Idem.*, *J. Mater. Soc, Japan*. **108** (1) (2000) 10.
20. H. P. KLUG and L. E. ALEXANDER, "X-ray Diffraction Procedures" (John Wiley, New York, 1974) Chap. 9.
21. D. AUTISSIER and L. AUTISSIEN, in Proceedings of ICF6. Tokyo, Japan, 1992, p. 132.
22. H. ROBBINS, in *Ferrites*, *Proc. Int. Conf.* (University of Tokyo, Tokyo, 1980) p. 7.
23. Z. X. TANG, C. M. SORENSEN, K. J. KLABUNDE and G. C. HADJIPANAYIS, *J. Colloid Interface. Sci.* **146** (1991) 38.

Received 22 November 1999
and accepted 2 November 2001